Solution combustion synthesis of CaZrO_3 ceramic perovskite using different fuels: In-situ FT-IR studies and monitoring of the flame reaction by thermocouple

P.-A. Goujon, Mohamed Mouyane, J. El Fallah, Jérôme Bernard, David Houivet

Open Ceramics 19 (2024) 100613

Contents lists available at ScienceDirect

Open Ceramics

journal homepage: www.sciencedirect.com/journal/open-ceramics

Solution combustion synthesis of $CaZrO_3$ ceramic perovskite using different fuels: *In-situ* FT-IR studies and monitoring of the flame reaction by thermocouple

P.-A. Goujon [a], M. Mouyane [a,*], J. El Fallah [b], J. Bernard [a], D. Houivet [a]

[a] Normandie Univ, Laboratoire Universitaire des Sciences Appliquées de Cherbourg (LUSAC), UNICAEN, LUSAC, EA 4253, France
[b] LCS- Laboratoire de Catalyse et Spectrochimie ENSICAEN-Université de Caen-CNRS, France

ARTICLE INFO

Handling Editor: Dr P Colombo

Keywords:
$CaZrO_3$ perovskite
Solution combustion synthesis
O/F ratio
Thermal decomposition
In situ TF-IR

ABSTRACT

In this study, nanoparticles of perovskite$CaZrO_3$ were prepared by a solution combustion technique using urea, glycine, β-alanineand citric acid as fuels. The aim of this work is to estimate the effect of these different fuels on the structure and microstructure of $CaZrO_3$ powders. The flame reaction was estimated by means of a thermocouple which allowed us to show that the combustion reaction velocity. The thermal decomposition of nitrate precursors was studied with the help of TG-DTA coupled with the infrared spectroscopy. The FT-IR spectroscopy enabled to check the identity of the evolved gases over the mass loss process. $CaZrO_3$ powders were calcined at 900 °C for 1 h. The powders were thoroughly characterized by scanning electron microscopy, X-ray diffraction andThermodilatometry. Also, the combustion process using glycine as fuel is beneficial to produce $CaZrO_3$ powders at low temperature, which are known to have a good reactivity with fine particles.

1. Introduction

Calcium Zirconate $CaZrO_3$ with a perovskite-type structure has been the object of many studies, due to its interesting physical properties. Calcium Zirconate, with a general formula of the form ABO_3 (where A is a large "divalent" cation and B is a small "tetravalent" cation), results from the combination of two compounds, namely CaO and ZrO_2. This compound shows a phase transition temperature from orthorhombic to cubic at 1750 °C [1]. At room temperature, deformed ZrO_6 establishes the orthorhombic structure (*Pbnm*). A thigh temperature, $CaZrO_3$ highlights the ideal cubic perovskite structure (*Pm3 m*) [2,3]. The $CaZrO_3$ oxide, when compared to other oxides, offers the possibility to prepare in the granular fine particle size. In addition, $CaZrO_3$ offers the possibility of being used as a ceramic material, due to its interesting properties such as high thermal stability, good chemical stability, high melting temperature (2345 °C), low thermal expansion coefficient, high strength and excellent corrosion resistance against alkali oxides [4,5]. In addition, this compound is suitable for various applications such as multilayer ceramic capacitors, humidity sensors, thermoelectric materials, refractory materials, high-temperature thermistor materials, catalyst materials, etc. [6,7]. $CaZrO_3$ is usually synthesized by solid state reaction at high temperature (1300–1450 °C) with a long calcination time, followed by a step of sintering process in the temperature range 1700–1800 °C [8]. In view of these parameters, the reaction in the solid state shows major drawbacks such as a large grain, low surface area, high agglomeration degree, inhomogeneity, etc. In addition, the high--temperature reaction causes volatility of certain atomic elements thus producing non-stoichiometry of the structure. In this regard, several methods have been used to achieve single-phase ceramic materials with fine particles, and with a high microstructural quality. To overcome these aforementioned drawbacks, intensive studies focused on the wet route which provides an alternative to solid state reaction. In this context, a number of alternative wet methods to prepare calcium zirconate ceramic powders have been described in the literature, such as sol-gel-combustion method [9], co-precipitation method [10,11], sol-gel reactions [12,13], hydrothermal synthesis [14,15], etc. Recently, a novel method has been developed for the synthesis of fine and pure calcium zirconate powders. This method is based on a wet-chemical technique, namely, "solution combustion synthesis" (SCS). This route allows to produce reactive material powders with high-purity, submicron grainsize in shorter time, high specific surface area and low temperature sinterability. In fact, submicron grains are characterized by a short diffusion distance between the components, which is beneficial for the reduction of both the calcination temperature and the holding time.

* Corresponding author.
E-mail address: mohamed.mouyane@unicaen.fr (M. Mouyane).

https://doi.org/10.1016/j.oceram.2024.100613
Received 22 November 2023; Received in revised form 14 May 2024; Accepted 23 May 2024
Available online 31 May 2024

The solution combustion synthesis is based on the use of highly exothermic redox chemical reactions between metals (nitrate precursors as oxidizers) and nonmetals (fuel as a reducer) [16–18]. Metals play the role of the cations and fuels are in the organic form. In the literature, urea [19], urea/citric acid mixture [20], glycine [21], β-alanine [7], citric acid [9] are used as fuels in the solution combustion synthesis of nano-scale $CaZrO_3$ powders. Prasanth et *al.* [20] reported that using urea with citric acid allows to produce the pure and uniform $CaZrO_3$ with a nanoparticle size of about 33 nm at 700 °C. The use of glycine enables to produce sing-phase ($CaZrO_3$ with particlesizesintherangeof30-90 nm [21]. The combustion powder (with glycine as a fuel) was calcined at 600 °C for3 hours. However, the use of citric acid and urea allows to elaborate $CaZrO_3$ powders with some defect and impurity [9,19]. Du et *al.* [9] reported that the use of citric acid as a fuel allows to produce single phasic nanosized $CaZrO_3$ and nanophosphor $CaZrO_3$:Eu^{3+} at low temperature (600 °C) with some impurity (ZrO_2). The grain size is about 50–100 nm. On the other hand, the synthesis of $CaZrO_3$:$Tb_{(0.03)}$ nanophosphor, by using urea at 1000 °C for 4 h, shows some cracks and porosity on the ceramic material. The author reported that the cause of these defects is an inhomogeneous heat and mass flow in the flame during the combustion process [9]. In addition, the XRD-analysis shows some intermediate phases at $2\theta = 30°$ [19]. Gonçalves et *al.* recently reported the adequacy and benefit of using β-alanine as a fuel in the synthesis of $CaZrO_3$ catalysts of high purity and crystallinity, without calcination step [7]. From these bibliographic data, we can note the key role played by the nature of the fuel used in the process, which certainly affects the quality of the synthesized powder. In fact, ignition and reaction temperature are affected by the nature of the fuel, and this will strongly influence the properties (phase composition and specific surface area) of the synthesized materials. On the other hand, Xanthopoulou et *al.* investigated the controllable combustion mode, by following the temperature evolution during the solution combustion synthesis of Ni/NiO nano-catalyst with glycine, and by using a thermocouple placed in and above the solution. They reported that an increasing amount of glycine in the initial mixture leads to a decrease in the maximum combustion temperature [22]. A number of publications about the preparation of calcium zirconate, by means of the solution combustion approach, are available [9,19,23]. However, no comparative study has been carried out so far in the case where different fuels are used. In addition, none of them reported about the synthesis of such a material in controllable combustion mode. Therefore, here we report about the synthesis of calcium zirconate by way of solution combustion synthesis, and by using four different fuels (citric acid, glycine, urea and β-alanine). The combustion temperature has been controlled through a thermocouple. The effect of the different fuels on the structure and microstructure of $CaZrO_3$ powders is discussed.

2. Experimental procedure

2.1. Thermal decomposition of (Zr, Ca) precursors

Before starting the synthesis of $CaZrO_3$, it is also necessary to have a clear idea of the evolved gas during the pyrolysis of the nitrate precursors ($Ca(NO_3)_2.4H_2O$ and $ZrO(NO_3)_2.\ xH_2O$). The decomposition gases evolved from the pyrolysis of (Zr, Ca) precursors was investigated using TG-DTA-IR. Thermogravimetric (TG) and differential thermal analyses (DTA) were performed in a Setaram 92–16.18 using alumina crucible between RT and 1200 °C at a heating rate of 10 $K.min^{-1}$ under air. TG measurement has been carried out by connecting the thermobalance to a FT-IR spectrometer (Model 730 by Nicolet USA). This has been done to analyze the gases evolved during the dehydration/decomposition processes. The measurements were performed up to 1200 °C at a heating rate of 10 $K.min^{-1}$ in atmospheric nitrogen (N_2) with a flow rate of 45 $mlmin^{-1}$. The IR-spectra of the evolved gases were obtained at 4 cm^{-1}resolution in the range 500-4000 cm^{-1}. The spectra were taken for 1.5 s at a frequency accuracy of 1 cm^{-1}.

2.2. Synthesis of $CaZrO_3$ with different fuels (urea, glycine, β-alanine and citric acid)

Calcium Zirconate oxide with a perovskite-type structure ($CaZrO_3$) was prepared by using the solution combustion synthesis. $Ca(NO_3)_2.4H_2O$ (99 %, Alfa Aesar) and $ZrO(NO_3)_2.\ xH_2O$ (99 %, Sigma-Aldrich)were used as the sources of Ca and Zr, respectively. Based on the TG analysis, the *x* value is equal to 7 (this value will be discussed in Section 3.1). So for the rest of the paper the zirconyl nitrate will be noted as $ZrO(NO_3)_2.7H_2O$.Urea $CO(NH_2)_2$ (99 %, Sigma-Aldrich), glycine $C_2H_5NO_2$ (99 %, Sigma-Aldrich), β-alanine $C_3H_7NO_2$ (99 %, Sigma-Aldrich) and citric acid $C_6H_8O_7$ (99 %, Prolabo) were used as fuels. Table 1 shows the semi-developed structural formulas of these fuel molecules. We can see that glycine and β-alanine are part of the series of the amino acids. The methyl group of β-alanine confers a certain thermal stability compared to glycine [24]. Urea exhibits two amino groups but citric acid contains a hydroxyl group and three carboxylic acid groups. The diversity of these fuel structural formulas can influence the SCS behavior. From these remarks, we are waiting to have a similar SCS behavior in the case of glycine and β-alanine [24].

The fuels are used as reducers and nitrate precursors are used as an oxidizer. Deionized water was used for preparing the solutions. The water content of the calcium and zirconium hydrates was determined by TG analysis. For $CaZrO_3$ composition, the concentration of the precursors in the solution was about 2.88 M of $Ca(NO_3)_2.4H_2O$ and 3.2 M of $ZrO(NO_3)_2.7H_2O$. The stoichiometric of fuel was calculated based on the oxidizer to fuel (urea or glycine or β-alanine or citric acid) ratio denoted by φ (O/F). The combustion reaction is strongly influenced by φ ratio. The value of φis calculated from the total oxidizing and reducing valencies. Some work report that the optimal stoichiometric conditions for combustion have been observed for $\varphi = 1$ [25]. In fact, at φ less than 1, the reaction solution is lean in fuel, however, at the higher φ ratio (>1), the fuel is in excess and the combustion reaction is complete. In this context, we have focused on the study of the effect of the nature of fuel on the combustion process with$\varphi = 1$. According to the concept of propellant chemistry, the oxidizing and reducing valencies of various elements used in the combustion process are considered as Ca = +2, Zr = +4, C = +4, H = +1, O = −2, N = 0, etc. Based on this concept, the oxidizing valencies of calcium nitrate and zirconium nitrate are −10 for each and the reducing valencies of urea, glycine, β-alanine and citric acid are +6, +9, +15 and + 18, respectively. The Fuel stoichiometric was calculated using $\varphi = O/F$ ratio. Accordingly, the molar ratio of 3.33, 3.22, 1.33 and 1.11 are used for urea, glycine, β-alanine and citric acid, respectively. These calculus values are given in Table 2.

Therefore, depending on the fuel used in the combustion process, the molar ratio between Zr-precursor and the fuel is varied. Thus, the molar ratio of nitrates:urea, nitrates:glycine, nitrates:β-alanine and nitrates: citric acid are 1:3.33, 1:2.22, 1:1.33 and 1:1.11, respectively. In a typical synthesis for the preparation of 0.03 mol $CaZrO_3$, the nitrate precursors and calculated amounts of fuel were dissolved separately in a minimum amount of deionized water in a 250 ml beaker at room temperature with continuous stirring using a magnetic stirrer. The nitrate solution with urea, glycine and citric acid highlights a milky white solution and the β-alanine form a limpid nitrate solution. The mixture was kept at 70 °C for 1 h until a clear viscous concentrated solution was obtained. Each clear transparent solution was transferred to an alumina crucible and placed into the stainless steel (inox 304) box with a lid which contained an opening. It is interesting to note that among the advantages of this material (inox 304) is high temperature resistance, easy to form and cost. The opening on the top lid permits the evacuation of gases and the passage of a thermocouple (N-type). The thermocouple permits to estimate the flash combustion temperature. The dimensions of the stainless-steel box are 140 mm width, 140 mm length and 80 mm height. The stainless-steel box with the solution is then introduced into a muffle furnace. The temperature is programmed to reach 550 °C with a free rise. The combustion velocity and the temperature of SCS process are

Table 1
Semi-developed structural formulas of urea, gycine, β-alanine and citric acid.

urea	glycine	β-alanine	citric acid
$H_2N-\underset{\underset{O}{\|}}{CH}-NH_2$	$H_2N-\underset{\underset{H}{\|}}{CH}-COOH$	$H_2N-\underset{\underset{CH_3}{\|}}{CH}-COOH$	$HOOC-\overset{\overset{COOH}{\|}}{\underset{\underset{OH}{\|}}{C}}-C-COOH$

measured by using N-type thermocouple (3 mm diameter and 500 mm length) which is placed above the stainless-steel box. After a few minutes an immediate exothermic reaction occurred. This can be related to a partial dehydration with a rapid evolution of large volumes of gases. When glycine and β-alanine are used as a fuel, the volume combustion takes places with voluminous and fluffy mass of oxide materials. However, when urea and citric acid are used, the combustion powder is not voluminous and is more agglomerated. This result agrees well with the similar structure formulas "amino acids" of both glycine and β-alanine (Table 1). On the other hand, with only amino groups (case of urea) or only carboxyl groups (case of citric acid), the SCS is not voluminous and no fluffy mass is observed for the powders. In all cases, the combustion is non-flaming due to the amount of fuels ($\varphi = \frac{O}{F} = 1$) used in the combustion process. The gas emissions observed during the combustion process are related to the release of nitrogen oxide, carbon dioxide and nitric acid gases as indicated by the following reactions (Eqs.1, 2, 3 and 4). Equations1, 2, 3 and 4 refer to the combustion reactions in which the fuels of urea, glycine, β-alanine and citric acid are used respectively, in the process. The gas emissions proposed in Eqs. 1, 2, 3 and 4are based on the IR spectroscopy data that followed the thermal decomposition of calcium nitrate and zirconyl nitrate as precursors (Section 3.1). The stoichiometric condition for all reactions is calculated assuming that the products are synthesized by excess of oxygen.

Eq.1 with urea:

$$Ca(NO_3)_2.4H_2O + ZrO(NO_3)_2.7H_2O + \frac{20}{6}CO(NH_2)_2 \rightarrow CaZrO_3 + \frac{106}{6}H_2O + \frac{20}{6}\,CO_2 + 4NO_x + \frac{40}{6}HNO_3$$

Eq.2 with glycine:

$$Ca(NO_3)_2.4H_2O + ZrO(NO_3)_2.7H_2O + \frac{20}{9}C_2H_5NO_2 \rightarrow CaZrO_3 + \frac{139}{9}H_2O + \frac{40}{9}CO_2 + 4NO_x + \frac{20}{9}HNO_3$$

Eq.3 with β-alanine:

$$Ca(NO_3)_2.4H_2O + ZrO(NO_3)_2.7H_2O + \frac{20}{15}C_3H_7NO_2 \rightarrow CaZrO_3 + \frac{225}{15}H_2O + \frac{60}{15}CO_2 + 4NO_x + \frac{20}{15}HNO_3$$

Eq.4 with citric acid:

Table 2
Oxidizing valencies of nitrate precursors "O", reducing valencies of fuel "F" and fuel stoichiometric $\varphi = \frac{|O|}{F}$. The oxidizing valencies of nitrate precursors is calculated by the sum of the oxidizing valencies of the calcium nitrate and zirconium nitrate. for each precursor, we have O = −10.

O	Nitrate precursors ($Ca(NO_3)_2.4H_2O$ and $ZrO(NO_3)_2.7H_2O$) −20			
F	urea +6	glycine +9	β-alanine +15	citric acid +18
$\varphi = \frac{\|O\|}{F}$	20/6 = 3.33	20/9 = 2.22	20/15 = 1.33	20/18 = 1.11

$$Ca(NO_3)_2.4H_2O + ZrO(NO_3)_2.7H_2O + \frac{20}{18}C_6H_8O_7 \rightarrow CaZrO_3 + \frac{241}{18}H_2O + \frac{120}{18}CO_2 + 1NO_x + 3HNO_3$$

The combustion product was then gently ground to powder in an agate mortar, giving white powders for urea, glycine and β-alanine. In contrast a black powder is obtained for citric acid. Probably this black powder is due to the amount of the carbon evolved during the SCS process which can be related to the structural formulas of citric acid with three carboxyl groups (Table 1). The general flowchart and schematic illustration for the combustion process are shown in Fig. 1. The ground combustion powders are then heated in air at 950 °C for 1 h.

2.3. Characterization methods

The apparatus and method of TG-DTA-IR have been described above

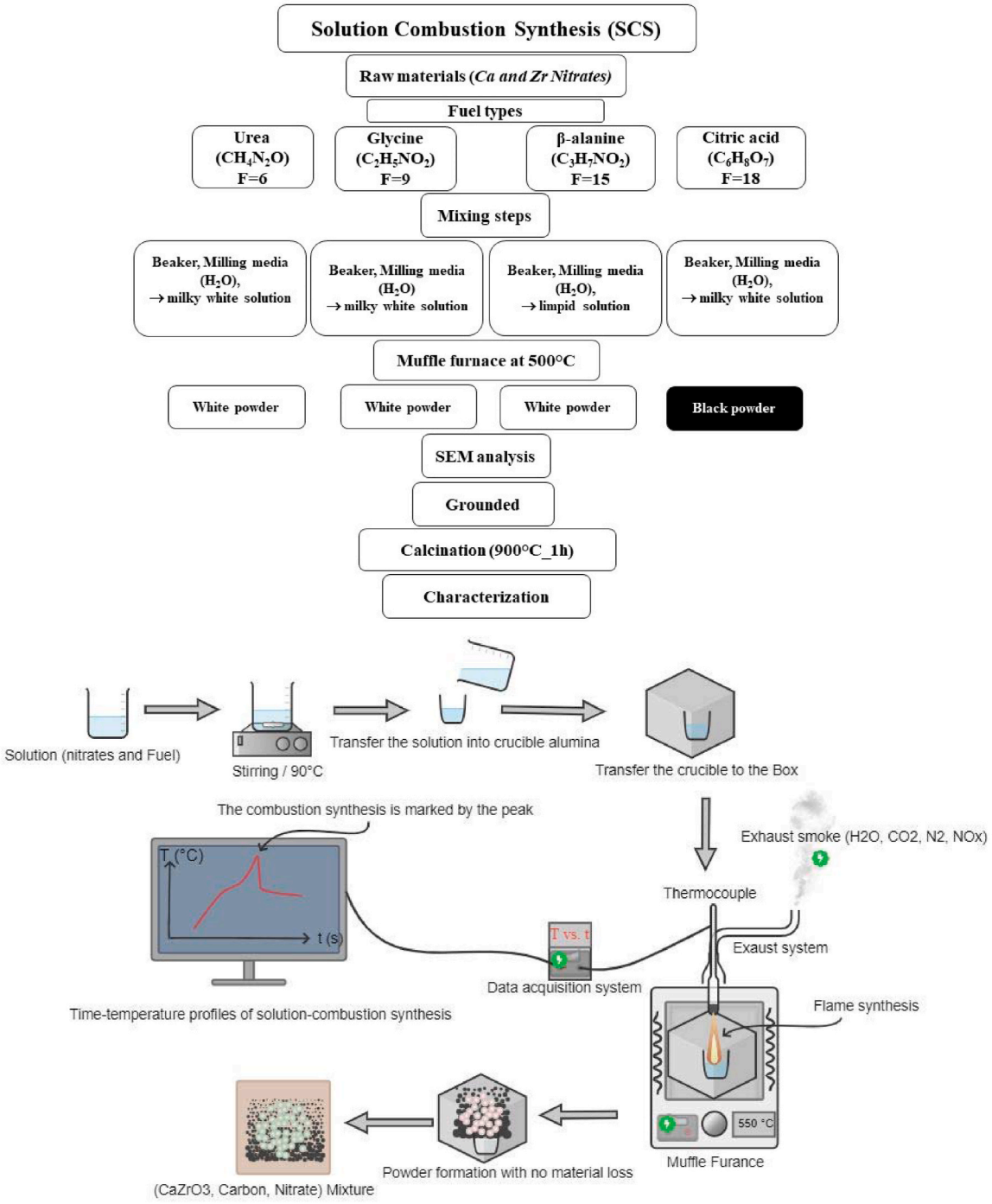

Fig. 1. (a) Experimental flowchart for the synthesis of $CaZrO_3$ by SCS with different fuels (b) Schematic illustration of SCS process. F: Fuels reducing valency.

in section 2.1. The XRD measurements were carried out at room temperature for the powders by using a PW1850 Philips diffractometer, employing a CuK_α radiation source ($\lambda = 1.540562$ Å) between 10 and 80° with a step size of 0.014° and a measuring time of 2 s at each step. X'pert Highscore was used for phase matching. In addition, the microstructural observations of the powders were performed by means of a Carl Zeiss Supra 55 high resolution scanning electron microscope (SEM, Hitachi S3400, Tokyo, Japan) in combination with energy dispersive spectrometer (EDS, Thermo Noran Middleton, WI, USA) analyzers. A Thermo-dilatometry analysis was performed in air up to 1550 °C with a Seteram TMA92, using a heating/cooling rate of 150 °C h^{-1}. The measurements were performed on the discs having a height of 10 mm and a diameter of 5 mm, obtained by pressing isostatically the powder at 196 MPa.

3. Results and discussion

3.1. Thermal decomposition of zirconyl nitrate and calcium nitrate

The thermal behavior of calcium nitrate and zirconyl nitrate as precursors of the solution combustion synthesis was studied with the help of TG-DTA in the temperature range of RT-1200 °C in static air. Fig. 2 shows the result of TG and DTA analysis of the nitrate precursors. $Ca(NO_3)_2.4H_2O$ and $ZrO(NO_3)_2.7H_2O$.In Fig. 2a, the DTA curve of

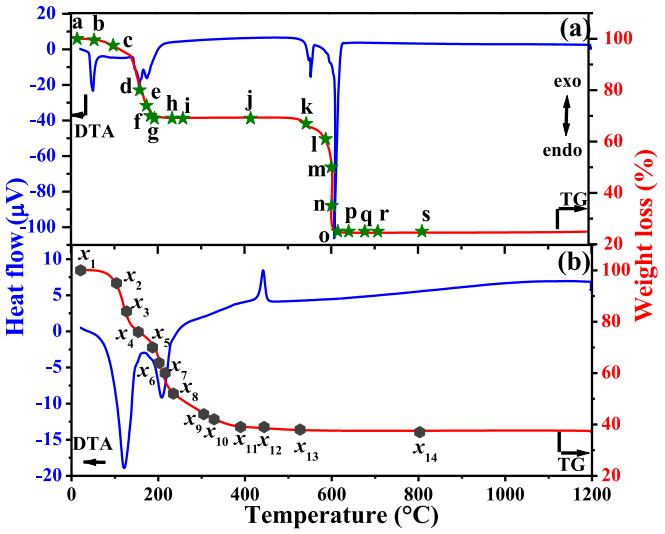

Fig. 2. TG-DTA of nitrate precursors in the range of 20–1200 °C. (a) Calcium nitrate, (b) zirconyl nitrate. Points (a) to (s) and (x_1) to (x_{14}) mark the samples, which were analyzed by IR spectroscopy for calcium nitrate and zirconyl nitrate, respectively.

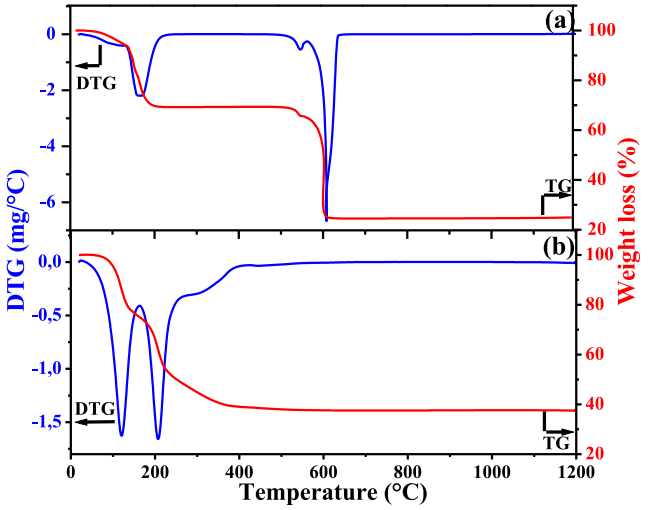

Fig. 3. TG-DTG profiles of nitrate precursors in the range of 20–1200 °C. (a) Calcium nitrate, (b) zirconyl nitrate.

calcium nitrate shows four endothermic peaks and the TG curve indicates a total weight loss of about 75 % up to 623 °C. These mass losses occur in two temperature regions. Furthermore, each region can be separated in two regions. The first weight loss (31 %) occurs in the 56–210 °C temperature range, accompanied with two endothermic peaks at 66 °C and at 166 °C. This process is accompanied by two distinct weight losses in TG/DTG profiles (see Fig. 3a). Each mass loss is associated with the release of the water adsorbed. The type of this molecule water will be discussed in section 3.2. About 4.17 mol of water were calculated considering the weight loss (31 %) observed in the first region. The difference of 0.17 mol of water was observed and this could be due to the hydration of the nitrate precursors. The second weight loss of 44 % appears from 515 to 623 °C, on two distinct steps in TG/DTG profiles (Fig. 3a), accompanied by two endothermic peaks (at 550 and at 617 °C), corresponding to the decomposition of organic residues and nitrates [26]. The differential thermal profile of $ZrO(NO_3)_2.7H_2O$ (Fig. 2b) shows only three peaks, two is endothermic and the third is exothermic which resulted in a total weight loss of 62 % in the range from RT to ~600 °C. These mass losses occur in three temperature regions and this was manifested by three distinct peaks in DTG (see Fig. 3b). The first weight loss (22.4 %) occurs in the 25–153 °C temperature range, accompanied by a large endothermic peak at 133 °C and is due to the volatilizations of the adsorbed water. The second loss of 25 % appears from 153 to 236 °C, accompanied with another endothermic peak at 214 °C, due to the decomposition of nitrates into amorphous ZrO_2 [27]. The third loss of 9 % manifested by a large overlap in DTG profile may be due to the complete decomposition of nitrates. This suggestion will be discussed in section 3.2. Another exothermic peak was observed at 450 °C that could be attributed to the formation of ZrO_2 tetragonal crystalline from the amorphous material [28]. Our results are consistent with previous results of Jadhav et al. [29]. The first weight loss of 35 % observed in the range temperature 25–200 °C is used to estimate the number of water molecules which correspond to $7H_2O$ per zirconyl nitrate. From these results, we can see that the thermal decomposition of calcium nitrate and the zirconyl nitrate occur in two different regions. The nitrate groups in the zirconyl decompose at low temperature, unlike those in the calcium nitrate which decompose at high temperature. These results will be discussed in section 3.2. Thus it can be concluded that calcium nitrate and zirconyl nitrate employed in this work are very likely $Ca(NO_3)_2.4H_2O$ and $ZrO(NO_3)_2.7H_2O$, respectively. Thus, the two thermal behaviors we can show that, at higher temperatures (>600 °C), no significant weight loss was observed, indicating that all the organic components were eliminated and that both oxides are stable.

3.2. FT-IR spectroscopy of zirconyl nitrate and calcium nitrate

In order to check the identity of the evolved gases over the mass loss process of calcium nitrate and zirconyl nitrate up to 800 °C, the TGA experiments were coupled with the FT-IR spectroscopy. The IR spectra as shown in Fig. 4. Fig. 4a show the IR absorption spectra of evolved gases from $Ca(NO_3)_2.4H_2O$ at different temperatures of the TG analysis. For clarity, nineteen points of all have been selected at 21, 60, 104, 165, 181, 190, 199, 240, 265, 421, 549, 594, 607, 608, 622, 647, 684, 714 and 816 °C. These temperatures correspond to the points marked by the letters (a) to (s) on the TG curve (see Fig. 2a). From Fig. 4a it can be seen that, at 21 °C (spectrum a), no IR absorption was detected, indicating the absence of evolved gases at this temperature. At 60 °C and104 °C (spectra b and c), only H_2O is produced during TG run (see the pointing bands at 4000-3400 and 2000-1300 cm^{-1}) [30,31]. This result agrees well with the first endothermic peak observed on the DTA curve and with the DTG profile. The analysis of spectra(d), (e), (f), (g) and (h) shows that the hydroxyl-stretching region located at 4000-3400 cm^{-1}, is shifted towards the lower wavenumbers than that centered at 3430 cm^{-1}. This broad asymmetric peak is due to the stretching mode of hydroxyl attached to calcium atoms. The spectrum obtained at 240 °C (h) displays a high absorption of the OH band. This result is in accordance with the TG-DTG/DTA data and can be correlated with the second endothermic peak observed on the DTA curve. Our results are similar to those presented in the literature [32]. At annealing temperatures of 264 (i) and 421 °C (j), no remaining signals of any organic constituents are observed, in accordance with the TG-DTG/DTA curves (Fig. 2a-3a). At 549 and 594 °C (k and l-spectra), significant contribution coming from nitrogen dioxide NO_2 (1650-1550 cm^{-1}) has appeared. This gas exhaust can be associated with the third DTA endothermic peak (Fig. 2a) and with the third weight loss observed on DTG curve (Fig. 3a). This range temperature consists of the first step of the main nitrate decomposition. From 607 °C (m), another nitrogen product was observed. In fact, in the temperature range 607 (m-spectrum) - 647 °C (p-spectrum), nitric acid (HNO_3) is highlighted by the appearance of three new absorption bands located at 750, 1260 and 1750 cm^{-1}. The q-spectrum at 684 °C shows that only the NO_2 absorption band is present, but no trace of the HNO_3 is detectable. The latter evolved gases correspond to the fourth weight loss which is associated with the endothermic phenomena in accordance

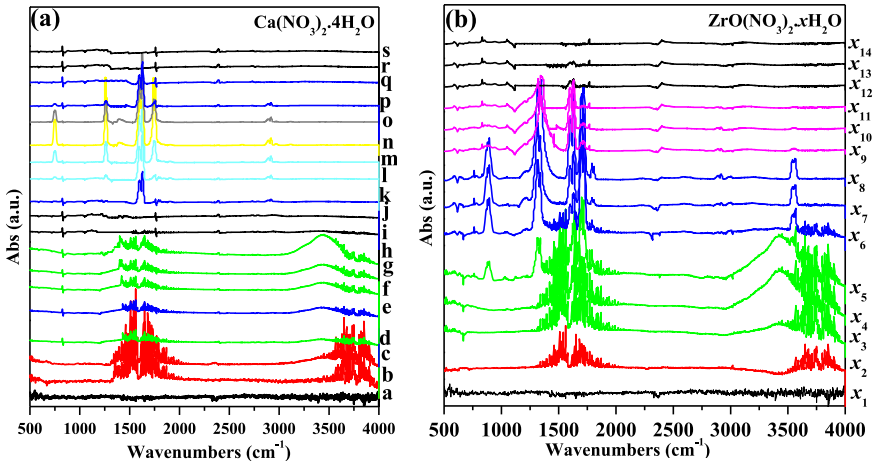

Fig. 4. IR spectra of the gases evolved at different temperatures during a TG run performed at 10 K min^{-1}on: (a) $Ca(NO_3)_2.4H_2O$ and (b) $ZrO(NO_3)_2.xH_2O$. Points (a) to (k)and (x_1) to(x_{11}) mark the samples, which were analyzed by IR spectroscopy, during TG run, for calcium nitrate and zirconyl nitrate, respectively. The main products detected are H_2O, N_2O and HNO_3.

Table 3
Chemical species evolved for $Ca(NO_3)_2.4H_2O$ and $ZrO(NO_3)_2.xH_2O$ at several temperatures.

Chemical species evolved	Decomposition temperatures range (°C)for:	
	$Ca(NO_3)_2.4H_2O$	$ZrO(NO_3)_2.xH_2O$
OH (H_2O)	60–104	104–202
OH linked group	165–240	127–187
No evolved gas	264–421	–
NO_2	549–684	187–390
HNO_3	607–647	187–235
No evolved gas	From 714	From 444

with the TG-DTG/DTA analysis. Finally, at high temperature (at 714 (r-spectrum) and 816 °C(s-spectrum) no gas is identified and in agreement with the result of TG-DTG, the reaction is finished. Thus, it seems that, and in accordance with TG-DTG/DTA data, the $Ca(NO_3)_2.4H_2O$ decomposed in fourth steps: the first two(from 60 to 240 °C)consist of the evolution of OH groups (free and linked), the third corresponds to the evolution of NO_2 gas in the temperature range of 549–684 °C and the fourth consists to the evolution of the HNO_3 in temperature range of 607–647 °C. These steps are summarized in Table 3.

The IR spectra of $ZrO(NO_3)_2.7H_2O$ is shown in Fig. 4b.Fourteentemperatures were chosen, in order to illustrate the decomposition profile of zirconyl nitrate. From this figure, we can see that the decomposition profile of zirconyl nitrate is different from that observed of calcium nitrate. In fact, the OH free group evolved from 104 (x_2) to 202 °C (x_6), whatever the evolution of OH linked group was observed on the x_3, x_4 and x_5-spectra in the temperature range of 127–187 °C. This result is in accordance with the TG-DTG/DTA data (Fig. 2b-3b) and with the weight loss used to estimate the number of water molecules which corresponds to $7H_2O$ per zirconyl nitrate ($7H_2O$ correspond to 35 % weight loss at 200 °C in TG curve). At 187 °C (x_5), we can note also that the evolution of OH groups (free and linked) is accompanied by the evolution of nitric acid (HNO_3). From 187 (x_5) to 235 °C (x_8) the evolving of nitrate groups (HNO_3 with NO_2) is observed. In addition, we also see that NO_2 has evolved up to 390 °C (x_{11}). This result is in good agreement with the TG data (Fig. 2b). Finally, at high temperature (at 444, 527 and 803 °C), for the spectra of (x_{12}), (x_{13}) and (x_{14}), respectively, no gas is identified and in accordance with TG-DTG curves, the reaction is finished. Thus, it seems that, and in accordance with TG-DTG/DTA data, the $ZrO(NO_3)_2.7H_2O$decomposes according to different overlapping stages. This result differs from that obtained of the calcium nitrates decomposition which shows four stages distinguished. These steps are summarized in Table 3. As shown in Table 3, we can note that, at 187 °C (x_5-spectra), the zirconyl nitrate was able to decompose into four amounts of OH (free and linked), NO_2 and HNO_3. Furthermore, Zr nitrate precursor decomposes at lower temperature to evolve NO_2 and HNO_3 amounts, in contrast the same decomposition was observed at high temperature for Ca nitrate precursor. In addition, the decomposition of Ca nitrate hydrate shows the evolution of OH amount (free and linked) at lower temperature which persists at higher temperature than those observed for Zr nitrate hydrate. As we can see from Table 3, at temperatures above 240 °C, the product corresponding to OH (free or linked) is not evolved in the case of Zr nitrate hydrate. Furthermore, as shown in Figs. 2 and 3, the temperature of 240 °C corresponds to the end of the dehydration process of the nitrate precursors. Moreover, N_2O is not detected during the thermal decomposition of both Ca and Zr nitrate precursors. The complete decompositions processes can be written as:

$$Ca(NO_3)_2.4H_2O \rightarrow CaO + \frac{7}{2}H_2O + NO_2 + HNO_3 + \frac{1}{4}O_2$$

$$ZrO(NO_3)_2.7H_2O \rightarrow ZrO_2 + \frac{13}{2}H_2O + NO_2 + HNO_3 + \frac{1}{4}O_2$$

In order to complete this study, the evolution of the individual gaseous species *vs.* temperature are plotted in Fig. 5. This data was constructed by the integration of the absorbance from IR spectra for OH free, OH linked, NO_2 and HNO_3 bands. The frequency value of each band is mentioned on Fig. 5. For Ca nitrate precursor, we can see that the formation of H_2O has occurred at a large temperature range (60–265 °C), however, the one of Zr nitrate precursor has been observed in the temperature range of 104–202 °C. On the other hand, an overlapping of nitrate decomposition and dehydration steps has been observed for Zr nitrate. Nevertheless, the 2 steps are well distinguished for Ca nitrate. This result is in accordance with TG-DTG/DTA analysis.

3.3. *In-situ monitoring of the SCS process as a function of fuel types*

In order to determine the combustion velocity during SCS process, the combustion temperature was monitored by using *in-situ* thermocouple. The typical temperature-time profile during the synthesis of $CaZrO_3$ by SCS using urea, glycine, β-alanine and citric acid is shown in Fig. 6. As shown in Fig. 6, a different thermal behavior was obtained depending on the fuel used during the synthesis. With β-alanine and glycine as fuels, the temperature profiles show clear exothermic peaks with ignition temperatures of 322 and 336 °C, respectively, and a maximum temperature of 635 and 593 °C are observed for the two fuels

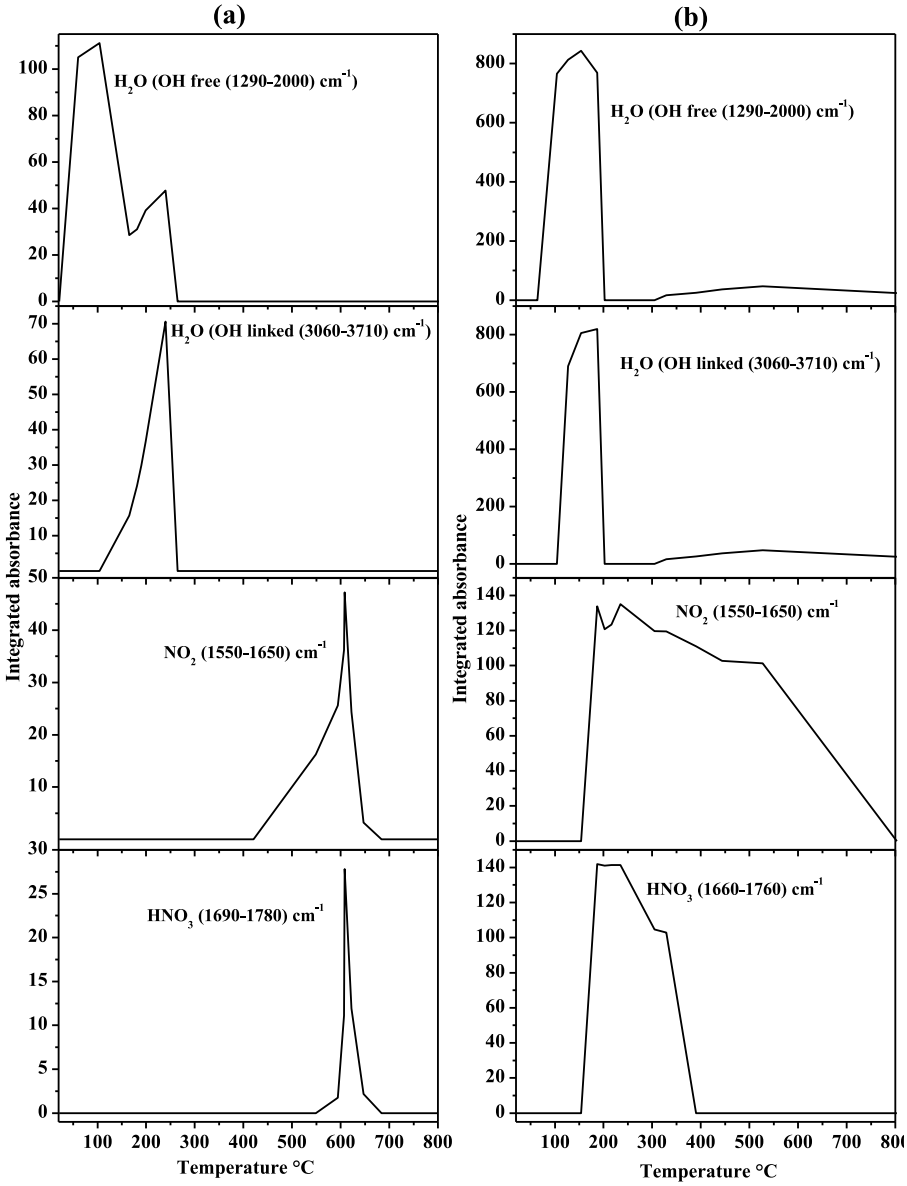

Fig. 5. Integration of IR-absorbance curves *vs.* temperature showing the evolution of gaseous species (H_2O, NO_2 and HNO_3) during the heating rate of 10 °Cmin^{-1}in the TG measurement. (a) $Ca(NO_3)_2.4H_2O$ and (b) $ZrO(NO_3)_2.xH_2O$.

in the previous order. This similar behavior may be related to the similar structural formulas of glycine and β-alanine (Table 1). However, the velocity of combustion reaction obtained in the case of β-alanine is slightly lower than that obtained for glycine. In this figure, we can also see that, citric acid and urea show that the combustion reactions take place slowly without any exothermic peak. This result is consistent with our microstructures powders, which show the voluminous and fluffy mass of oxide materials. In addition, except citric acid, all combustibles highlight a drop-in temperature profiles at about 200 °C after that the combustion reactions take place. This drop can be related at an endothermic reaction due to due to volatilizations of the water adsorbed and some nitrate decomposition. It is important to remember that at 200 °C, the water is released along with the decomposition of Zr nitrate (see Fig. 5). This result agrees with the TG-DTG/DTA curves of nitrate precursors (Figs. 2 and 3). In fact, there is a correlation between TG-DTG/DTA data and *in situ* FT-IR spectra.

3.4. Structural and microstructural analysis

3.4.1. Phase purity

The XRD patterns of $CaZrO_3$ synthesized by SCS using different fuels are presented in Fig. 7. The phase purity in the as-burnt powders and post annealed powders, obtained with different fuels is discussed separately. As shown in Fig. 7a, the synthesis with glycine allows to obtain a pure and well crystallized $CaZrO_3$. The observed Bragg reflections in the XRD patterns obtained for glycine as a fuel were indexed according to the standard powder diffraction data of $CaZrO_3$ in the JCPDS file #35–0790. However, the XRD patterns of β-alanine combustion (Fig. 7b) show crystallized $CaZrO_3$ phase with some crystal diffraction peaks at $2\theta = 30.20°$ (marked with star) which corresponds to the ZrO_2 phase. This impurity peak may be caused by ZrO_2 or precursors that did not react completely during the combustion process [33]. When urea or citric acid (Fig. 7c and d, respectively)were used as a fuel, the XRD patterns show the amorphous material of $CaZrO_3$ phase. These differences of the as-burnt powders XRD patterns is due to the fact that the combustion wave is not uniform and depends on the fuels used in the

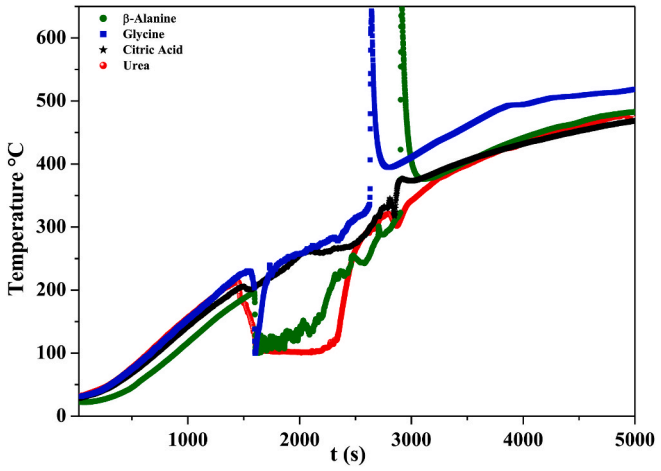

Fig. 6. Temperature-time profile during the synthesis of $CaZrO_3$ by SCS using urea, glycine, citric acid and β-alanine.

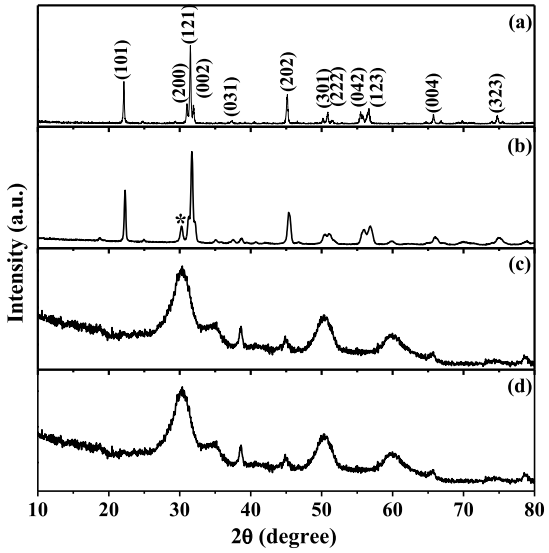

Fig. 7. XRD patterns of $CaZrO_3$ powders derived from solution combustion synthesis using four fuels: (a) glycine, (b) β-alanine, (c) urea, and (d) citric acid fuels.

SCS process. This result agrees with the temperature-time profile (Fig. 6) of the combustion reaction with different fuels which indicate that the strong combustion reaction in the case of glycine and β-alanine is considerably greater than those observed for urea and citric acid fuels. The strong combustion reaction is evidenced by an intense peak on the temperature-time profile (Fig. 6). These results clearly show the effectiveness of glycine as a fuel in SCS process to produce cleaner and well crystallized powders.

X-ray diffraction patterns of the $CaZrO_3$ powders obtained by SCS followed by a heat treatment at 900 °C for 1 h in air are shown in Fig. 8. The letters a-b refer to the glycine, β-alanine, urea, and citric acid, respectively.

It can be seen that the diffractograms show the same patterns indicating the single formation of $CaZrO_3$ perovskite phase. However, the XRD patterns of as-powders also show the additional peaks which can be attributed to theZrO_2 impurity and which are more marked with urea (Fig. 8c).

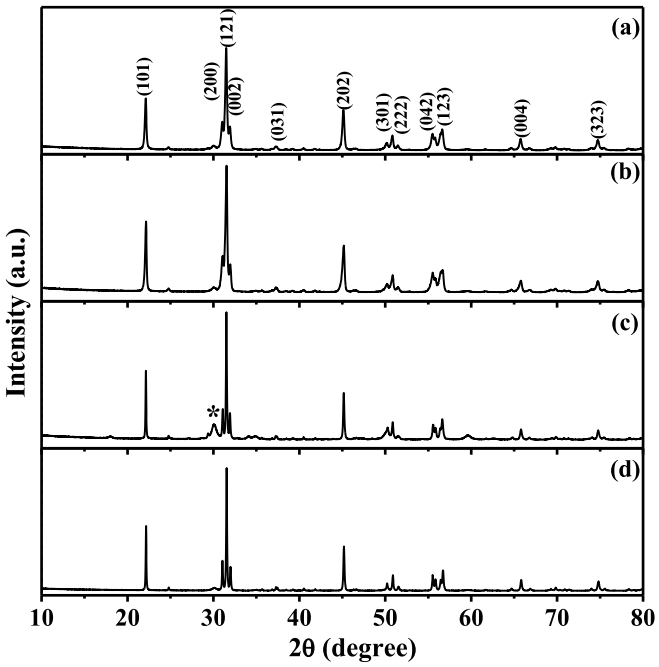

Fig. 8. XRD patterns of $CaZrO_3$ powders derived from solution combustion synthesis using different fuels followed by a heat treatment at 900 °C for 1 h in air: (a) glycine, (b) β-alanine, (c) urea, and (d) citric acid fuels.

3.4.2. *Morphology and crystallite size*

A complete microstructural analysis was recorded on the all non-treated perovskite powders obtained by SCS process. The SEM micrographs of $CaZrO_3$ powders obtained by using different fuels are shown in Fig. 9. From this figure, it can be seen that the micrographs highlight $CaZrO_3$ nanoparticles of the glycine,β-alanine and citric acid combustion products as shown in Figs. (9a), (9b) and (9c). These later samples also show a fluffy foam with porous structure which can be attributed to a release of a large volume of gases during the combustion process (H_2O, NO_2, HNO_3 and CO_2). This result is in accordance with the previous research [16,17]. However, the images obtained on the as-prepared samples by glycine and β-alanine (Fig. 9a and b) clearly indicate that a transparent veil-like film was encapsulated around $CaZrO_3$ nanoparticles. The high-magnification images of Fig. 9a and b shows that the particles have a round shape with an average size of about 60 nm. The average size of citric acid-combustion particles deduced from the SEM photograph (Fig. 9d) is about 130 nm. On the other hand, the SEM data in Fig. 9c shows that the urea-combustion sample shows a dense microstructure and the particle size is not estimated.

Whatever the fuel employed in the SCS process, the atomic percentages derived from the EDS spectra of all the combustion powders (Table 4) clearly indicated that all samples contain Ca, Zr and O elements and also showed that the cationic composition has a Ca:Zr ratio of about 1:1 suggesting the purity of the product synthesized.

3.5. *Thermo-dilatometry*

Fig. 10 shows the thermo-dilatometric measurements up to1550 °C in air for the $CaZrO_3$ ceramic powders. The study was carried out on the non-annealed samples. Our choice is based on the XRD data (Fig. 7) of the samples obtained by combustion that show crystallized phase of $CaZrO_3$ of glycine and of β-alanine. The maximum shrinkage of 27–28 % is obtained for both glycine and citric acid powders, while the urea-sample shows a minimum (14 %). The dilatometric curve recorded on the citric acid sample shows two distinct sintering steps. The first one occurs in the 500–900 °C temperature range with a shrink of about 6 % and the second one appears from 900 to 1500 °C with a shrink of about

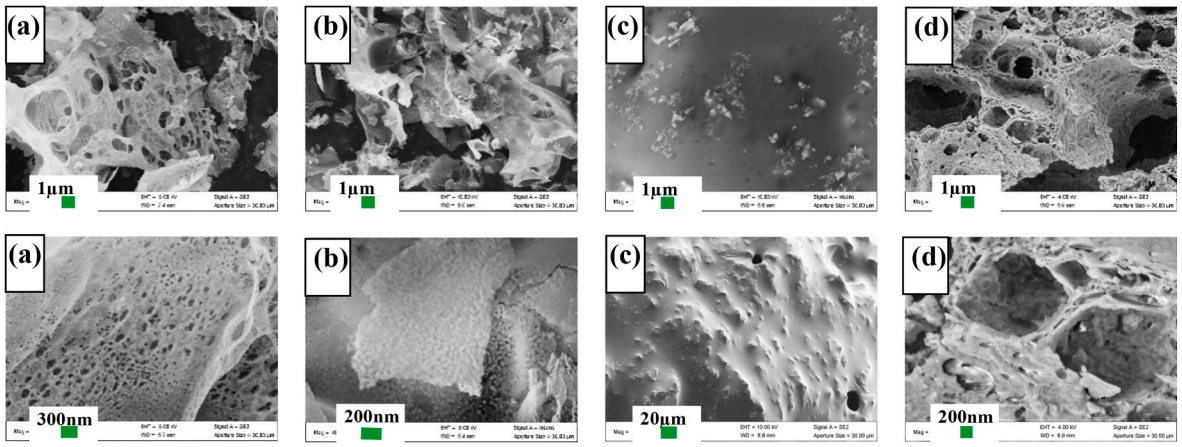

Fig. 9. SEM micrographs of non-treated $CaZrO_3$ powders derived from solution combustion synthesis using different fuels. (a, b, c and d refer to glycine,β-alanine, urea and citric acid, respectively).

Table 4
Atomic percentages obtained from EDS analyses of the all combustion powders.

Investigated powder in the SEM image	% atomic		
	Ca	Zr	O
glycine	11.39 ± 0,17	11,66 ± 0,14	76,95 ± 1,41
β-alanine	18,54 ± 0,13	18,37 ± 0,11	63,09 ± 0,88
citric acid	19,93 ± 0,15	19,63 ± 0,12	60,08 ± 1,01
urea	17,73 ± 0,14	17,27 ± 0,11	65 ± 0,92

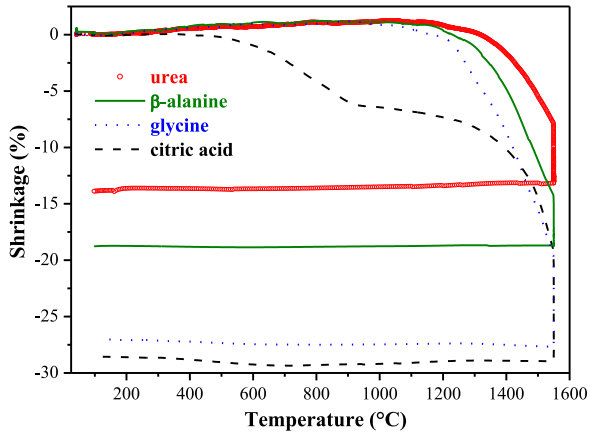

Fig. 10. Shrinkage curve of $CaZrO_3$ samples derived from SCS process using different fuels as a function of temperature. (a, b, c and d refer to glycine, β-alanine, urea and citric acid, respectively).

14 %. The first step corresponds probably to a formation of the necks between the $CaZrO_3$ particles during the sintering stage, whereas the second step highlights densification rate. However, only one sintering step was observed on the other three samples (urea, β-alanine and glycine). Another important observation is that the sintering behavior of glycine, β-alanine and urea samples starts at 1200, 1300 and 1330 °C, respectively. It can also be seen that the sintering step (the second step) of the citric acid sample starts around 1400 °C.However, the end of sintering for all the samples is greater than 1550 °C.The results indicate that the combustion process with a fuel like glycine is beneficial to produce the $CaZrO_3$ precursor powder at low temperature which has good reactivity with fine particles.

4. Conclusion

A low-cost solution combustion synthesis from nitrate precursors has been used to synthesizenanosized$CaZrO_3$ powders. However, the use of different fuels (urea, glycine, β-alanineor citric acid) allows different behaviours of the combustion reaction. Here, we demonstrate that with glycine and β-alanine, the behavior is similar with the presence of the marked exothermic peaks, which means that the reactions are strong. The flame reaction was estimated by using a thermocouple which shows that the combustion reaction velocity depends on the fuel used and that the highest rate is obtained in the case of glycine and β-alanine. This similar thermal behavior may be related to the structural formulas of glycine and β-alanine. The results indicate that the combustion process with a fuel like glycine is beneficial to produce the $CaZrO_3$ precursor powder at low temperature which has good reactivity with fine particles.

On the other hand, calcium nitrate decomposes on heating in two distinct stages: the first concerns the decomposition of OH groups and the second consists of gaseous releases of NO_2 and HNO_3. However, zirconyl nitrate decomposes at a lower temperature into OH groups, NO_2 and HNO_3. These evolved gases occur at overlapping stages.

CRediT authorship contribution statement

P.-A. Goujon: Data curation. **M. Mouyane:** Writing – review & editing, Writing – original draft, Supervision, Writing – review & editing, Writing – original draft, Supervision. **J. El Fallah:** Formal analysis. **J. Bernard:** Validation. **D. Houivet:** Supervision.

Declaration of competing interest

The authors declare that they have no known competing financial interests or personal relationships that could have appeared to influence the work reported in this paper.

References

[1] W.D. Macedo Jr., A.E. Souza, G.T.A. Santos, S.R. Teixeira, E. Longo, Microwave-assisted hydrothermal synthesis followed by heat treatment: a new route to obtain $CaZrO_3$, Ceram. Int. 44 (2018) 953–958.
[2] H.J.A. Koopmans, G.M.H. van de Velde, P.J. Gellings, Powder neutron diffraction study of the perovskites $CaTiO_3$ and $CaZrO_3$, Acta Crystallogr. C39 (1983) 1323–1325.

[3] Z.F. Hou, Ab initio calculations of elastic modulus and electronic structures of cubic $CaZrO_3$, Physica B 403 (2008) 2624–2628.

[4] J. Szczerba, Z. Pedzich, The effect of natural dolomite admixtures on calcium zirconate-periclase materials microstructure evolution, Ceram. Int. 36 (2010) 535–547.

[5] P. Stoch, J. Szczerb, D.M.J. Lis, Z. Pedzich, Crystal structure and ab initio calculations of $CaZrO_3$, J. Eur. Ceram. Soc. 32 (2012) 665–670.

[6] C.C. Wang, S.A. Akbar, W. Chen, J.R. Schorr, High-temperature thermistors based on yttria and calcium zirconate, Sensor. Actuator. A58 (1997) 237–243.

[7] A.M. Gonçalves, R.A.B. Lima-Corrêa, J.M. Assaf, A.R.A. Nogueira, Lithium and calcium based perovskite type oxides for ethylic transesterification, Catal. Today 279 (2017) 177–186.

[8] V.P. Gorelov, V.B. Balakireva, A.V. Kuz'min, Partial conductivities in perovskites $CaZr_{1-x}Sc_xO_{3-\alpha}$ (x=0.03-0.20) in an oxidation atmosphere, Phys. Solid State 58 (2016) 12–18.

[9] Q. Du, G. Zhou, J. Zhou, H. Zhou, Combustion synthesis and photoluminescence properties of $CaZrO_3:Eu^{3+}$ with highly enhanced brightness by Li^+ doping, J. Lumin. 137 (2013) 83–87.

[10] L. van Rij, L. Winnubst, L. Jun, J. Schoonman, Analysis of the preparation of Indoped$CaZrO_3$ using a peroxo-oxalate complexation method, J. Mater. Chem. 10 (2000) 2515–2521.

[11] M. Dudek, E. Drożdż-Cieśla, Some observations on synthesis and electrolyticproperties of nonstoichiometric calcium zirconate, J. Alloys Compd. 475 (2009) 846–854.

[12] J. Han, Z. Wen, J. Zhang, X. Xu, Z. Gu, Y. Liu, Synthesis and characterization of proton conductive $CaZr_{0.90}In_{0.10}O_{3-\delta}$ by a citric acid complexation method, Fusion Eng. Des. 85 (2010) 2100–2104.

[13] M. Zhou, A. Ahmad, Sol-gel processing of In-doped $CaZrO_3$ solid electrolyte and the impedimetric sensing characteristics of humidity and hydrogen, Sens. Actuators, B 129 (2008) 285–291.

[14] M. Dudek, A. Rapacz-Kmita, CaZrO3-based powders suitable for manufacturing electrochemical oxygen probes, Cent. Eur. J. Chem. 11 (2013) 2088–2297.

[15] Sh M. Khaliullin, V.D. Zhuravlev, V.G. Bamburov, L.V. Ermakova, Synthesis of submicron $CaZrO_3$ in combustion reactions, Phys. At. Nucl. 78 (2015) 1382–1388.

[16] M. Mouyane, B. Jaber, B. Bendjemil, J. Bernard, D. Houivet, J.G. Noudem, Sintering behavior of magnesium aluminate spinel $MgAl_2O_4$ synthesized by different methods, Int. J. Appl. Ceram. Technol. 16 (2019) 1138–1149.

[17] M. Mouyane, B. Itaalit, J. Bernard, D. Houivet, J.G. Noudem, Flash combustion synthesis of electron doped-CaMnO3 thermoelectric oxides, Powder Technol. 264 (2014) 71–77.

[18] I. Zahwa, M. Mouyane, A. Kassas, A.N. Kamlo, C. Moslah, J. Navas, S. Livraghi, J. Bernard, J. El Falah, J. Toufaily, T. Hamieh, D., Flash combustion synthesis using two different fuels and characterization of LiF-doped TiO_2 for the photocatalytic applications, Open Ceramics 17 (2024) 100562.

[19] V. Singh, S. Watanabe, T.K. Gundu Rao, K. Al-Shamery, M. Haase, Y.-D. Jho, Synthesis, characterisation, luminescence and defect centres in solution combustion synthesized $CaZrO_3:Tb^{3+}$ phosphor, J. Lumin. 32 (2012) 2036–2042.

[20] C.S. Prasanth, H. Padma Kumar, R. Pazhani, Sam Solomon, J.K. Thomas, Synthesis, characterization and microwave dielectric properties of nanocrystalline CaZrO3 ceramics, J. Alloys Compd. 464 (2009) 306–309.

[21] K. Boobalan, A. Varun, R. Vijayaraghavan, K. Chidambaram, U.K. Mudali, Facile, scalable synthesis of nanocrystalline calcium zirconate by the solution combustion method, Ceram. Int. 40 (2014) 5781–5786.

[22] G. Xanthopoulou, O. Thoda, S. Roslyakov, A. Steinman, D. Kovalev, E. Levashov, G. Vekinis, A. Sytschev, A. Chroneos, Solution combustion synthesis of nano-catalysts with a hierarchicalstructure, J. Catal. 364 (2018) 112–124.

[23] R. Ianos, P. Barvinschi, Solution combustion synthesis of calcium zirconate, $CaZrO_3$, powders, J. Solid State Chem. 183 (2010) 491–496.

[24] V. Ya Yablokov, I.L. Smel'tsova, I.A. Zelyaev, S.V. Mitrofanova, Studies of the rates of thermal decomposition of Glycine, alanine, and serine, Zh. Obshch. Khim. 79 (2009) 1704–1706.

[25] C.-H. Jung, S. Jalota, S.B. Bhaduri, Quantitative effects of fuel on the synthesis of Ni/NiO particles using a microwave-induced solution combustion synthesis in air atmosphere, Mater. Lett. 59 (2005) 2426–2432.

[26] N.P. Bansal, Low temperature synthesis of calcia±silica glasses having stable liquid-liquid immiscibility by the sol-gel process, J. Mater. Sci. 27 (1992), 2992-2933.

[27] N.P. Bansal, Low temperature synthesis of CaO-SiO_2 glasses having stable liquid-liquid immiscibility by the sol-gel process, J. Mater. Sci. 27 (1992) 2922–2933.

[28] C.Y. Tai, B.-Y. Hsiao, H.-Y. Chiu, Preparation of silazane grafted yttria-stabilized zirconia nanocrystals via water/CTAB/hexanol revers microemulsion, Mater. Lett. 61 (2007) 834–836.

[29] L.D. Jadhav, A.P. Jamale, S.R. Bharadwaj, S. Varma, C.H. Bhosale, Synthesis and characterization of YSZ by spray pyrolysis technique, Appl. Surf. Sci. 258 (2012) 9501–9504.

[30] G.F. de Oliveiraa, R.C. de Andradeb, M.A.G. Trindadea, H.M.C. dradeb, C.T. d. Carvalho, Thermogravimetric and spectroscopic study (TG-DTA/FT-IR) of activated carbon from the renewable biomass source babassu, Quim. Nova 40 (2017) 284–292.

[31] J. Li, Z. Wang, X. Yang, L. Hu, Y. Liu, C. Wang, Evaluate the pyrolysis pathway of glycine and glycylglycine by TG-FTIR, J. Anal. Appl. Pyrolysis 80 (2007) 247–253.

[32] J.C.A.A. Roelofs, J.A. van Bokhoven, A.J. van Dillen, J.W. Geus, K.P.d. Jong, The thermal decomposition of Mg-Al hydrotalcites: effects of interlayer anions and characteristics of the final structure, J. Chem. Eur. 8 (2002).

[33] Q. Du, G. Zhou, J. Zhou, H. Zhou, Combustion synthesis and photoluminescence properties of $CaZrO_3:Eu^{3+}$ with highly enhanced brightness by Li^+ doping, J. Lumin. 137 (2013) 83–87.